

## Understanding and revisiting the most complex perovskite system via atomistic simulations

Yali Yang,<sup>1,2</sup> Bin Xu,<sup>2</sup> Changsong Xu,<sup>2</sup> Wei Ren,<sup>1,2,\*</sup> and Laurent Bellaïche<sup>2,†</sup>

<sup>1</sup>International Centre for Quantum and Molecular Structures, Physics Department, Shanghai University, Shanghai 200444, China

<sup>2</sup>Physics Department and Institute for Nanoscience and Engineering, University of Arkansas, Fayetteville, Arkansas 72701, USA



(Received 3 March 2018; published 29 May 2018)

A first-principles-based effective Hamiltonian is developed and used, along with direct *ab initio* techniques, to investigate finite-temperature properties of the system commonly coined the most complex perovskite, that is  $\text{NaNbO}_3$ . Such simulations successfully reproduce the existence of seven different phases in its phase diagram. The decomposition of the total energy of this effective Hamiltonian into different terms, altogether with the values of the parameters associated with these terms, also allow us to shed some light into puzzling features of such a compound. Examples include revealing the microscopic reasons of why  $R3c$  is its ground state and why it solely adopts in-phase tiltings at high temperatures *versus* complex nanotwins for intermediate temperatures. The results of the computations also call for a revisiting of the so-called  $P$ ,  $R$ , and  $S$  states, in the sense that an unexpected and previously overlooked inhomogeneous electrical polarization is numerically found in the  $P$  state while complex tiltings associated with the simultaneous condensation of *several*  $k$  points are predicted for the controversial  $R$  and  $S$  phases.

DOI: [10.1103/PhysRevB.97.174106](https://doi.org/10.1103/PhysRevB.97.174106)

### I. INTRODUCTION

$\text{ABX}_3$  (where  $X$  are, e.g., O or F ions) perovskites constitute an important family of materials since it can exhibit various important phenomena, such as ferroelectricity, magnetism, multiferroicity, and superconductivity (see, e.g., Refs. [1–5] and references therein). Out of all the perovskites known to date, a particular one has been dubbed the most complex perovskite system [5], which is  $\text{NaNbO}_3$ . Such a compound has been extensively studied during the past decades, partly because of its optical property [6] and its design as high output piezoelectric nanogenerator (when grown in nanowires' form) [7] but also because of the possibility to generate lead-free materials having large piezoelectricity when mixed with  $\text{KNbO}_3$  [8–11].  $\text{NaNbO}_3$  owes its nickname to the unusual large number of states appearing in its phase transition sequence when varying the temperature [12–14]. As a matter of fact, it is commonly accepted that  $\text{NaNbO}_3$  has seven major phases with the highest temperature state being cubic ( $Pm\bar{3}m$ , above 913 K) and being typically denoted as  $U$ . Upon cooling down, this material undergoes a sequence of phase transitions which were introduced in the classic work of Megaw *et al.* in 1974 [14] as: tetragonal  $T_2$  phase ( $P4/mbm$ , 913–848 K), orthorhombic  $T_1$  phase ( $Cmcm$ , 848–793 K), orthorhombic  $S$  phase ( $Pmmn$ , 793–753 K), orthorhombic  $R$  phase ( $Pmmn$ , 753–633 K), orthorhombic  $P$  phase ( $Pbcm$ , 633–173 K), and finally rhombohedral  $N$  phase ( $R3c$ , below 173 K).

However, controversies still exist nowadays about such a sequence and some of these phases. For instance, an additional room temperature  $Q$  state of  $Pmc2_1$  symmetry was suggested to coexist with the  $P$  phase in some  $\text{NaNbO}_3$  samples,

depending on their processing (such coexistence arises from the proposed first-order nature of the transition between these  $P$  and  $Q$  phases [15–17]). Similarly, a novel monoclinic structure with  $Pm$  symmetry was proposed at ambient temperature in Ref. [18], and an original quantum paraelectric phase was even suggested below 200 K [19]. Moreover, new refined solutions for the  $R$  and  $S$  phases can further be found in the literature. For example,  $R$  and  $S$  phases of  $Pbnm$  symmetry were given by Mishra *et al.* based on a high-resolution powder neutron diffraction study [12], while Peel *et al.* proposed two possible structural models for the  $R$  phase between 643 K and 743 K: one being of  $Pbnm$  symmetry while the other is of  $Pmmn$  space group, with each of these two solutions having a  $2 \times 2 \times 6$  periodic cell and differing only by the nature of the complex tilt system along the long axis. The difficulty of fully characterizing these  $R$  and  $S$  phases likely mostly resides, in fact, in the challenging task of determining their precise complex and long-period tilting pattern of the oxygen octahedra along some particular axis.

Several first-principles studies have been carried out in the past to better understand  $\text{NaNbO}_3$  (see, e.g., Refs. [20–22]). However, the fact that *ab initio* simulations are typically performed at zero Kelvin and on small supercells renders the task of, e.g., determining the precise transition sequence and the characterization of complex phases (such as  $R$  and  $S$ ) dantesque or can even thought to be impossible. On the other hand, shedding light into the complexity of  $\text{NaNbO}_3$  via the use of first-principles-based atomistic schemes (such as effective Hamiltonian approaches [23–26], bond valence models [27–29], shell models [30–32], or all-ions “second principles” techniques [33,34]) rather than direct first-principles techniques can still be hoped, especially once recalling that such schemes naturally incorporate temperature effects as well as are able to treat rather large supercells. Moreover, effective Hamiltonians have led to remarkable successes in handling

\*Corresponding author: [renwei@shu.edu.cn](mailto:renwei@shu.edu.cn)

†Corresponding author: [laurent@uark.edu](mailto:laurent@uark.edu)

rather complex issues in the past, such as (1) confirming the existence of a monoclinic phase in  $\text{Pb}(\text{Zr},\text{Ti})\text{O}_3$  (PZT) that was experimentally discovered for a narrow range of Ti compositions [35], and providing a successful explanation for a long-standing problem, namely why ceramics of PZT exhibit a so large piezoelectric response [25], and (2) reproducing and understanding [36] the striking nanostripes experimentally found in ultrathin films [37,38], as well as, leading to predictions of novel phenomena—such as ferroelectric vortices [39] and bubbles [40] that were then experimentally confirmed more than 10 years later after the predictions [41,42]. However, it is the authors' belief that being able to demonstrate that atomistic simulations are able to reproduce the various numerous phases of  $\text{NaNbO}_3$  and capture the unusual complexity of this system is probably the most challenging test ever asked of them. In other words, succeeding in doing so will put such simulations at a new and unprecedented predictive level, in addition to provide a novel probe into this complex system.

The goal of this paper is to build and employ an effective Hamiltonian scheme for  $\text{NaNbO}_3$ , and to indeed demonstrate that such a technique does reproduce the existence of seven important phases in the phase diagram of this material. It even provides solutions for the  $R$  and  $S$  phases that emerge from the simultaneous condensation of several  $k$  points (rather than a unique one) and that result in rather complex tilting patterns. Strikingly, the use of this effective Hamiltonian, and the confirmation by additional direct first-principles calculations we further performed, also call for a revisiting of the  $P$  phase. Finally, the decomposition of the total energy of this effective Hamiltonian into several different terms is presently found to be rather useful for the quest of understanding specific features that make  $\text{NaNbO}_3$  unique and worthy of its nickname of the most complex perovskite system.

The paper is organized as follows. Section II reports in details the developed effective Hamiltonian and its parameters, as well as details about direct *ab initio* computations employed here. Sections III A and III B give and analyze in length results at small and finite temperatures, respectively. Section IV provides a discussion aimed at better understanding  $\text{NaNbO}_3$  by pointing out specific interactions as well as the sign and magnitude of parameters characterizing the strength of these interactions. Finally, Sec. V concludes this paper.

## II. METHODS

### A. Effective Hamiltonian

Here, we develop an effective Hamiltonian ( $H_{\text{eff}}$ ) to mimic and understand properties of  $\text{NaNbO}_3$  bulk. It has four degrees of freedoms, namely (1) the Na-centered local soft mode  $\mathbf{u}_i$ , which is directly proportional to the electric dipole of the 5-atom cell  $i$ ; (2) the homogenous strain tensor,  $\{\eta_l\}$ ; (3) the Nb-centered dimensionless variable  $\mathbf{v}_i$ , that is related to the inhomogeneous strain within the 5-atom cell  $i$  [26] (note that the total strain, that includes both homogeneous and inhomogeneous contributions, will be denoted here as  $\eta_l$  and will be expressed using the Voigt notation, and that the zero of strain corresponds to the equilibrium 0 K cubic state of  $\text{NaNbO}_3$ ); and (4) the Nb-centered pseudovector  $\boldsymbol{\omega}_i$  that quantifies oxygen octahedral tiltings [43] (also commonly

termed antiferrodistortive (AFD) distortions) in the 5-atom unit cell  $i$ . For instance,  $\boldsymbol{\omega}_i = 0.1(\mathbf{x} + \mathbf{y} + \mathbf{z})$ , where  $\mathbf{x}$ ,  $\mathbf{y}$ , and  $\mathbf{z}$  are the unit vectors along the  $x$ ,  $y$ , and  $z$  axes (that are aligned along the pseudocubic [100], [010], and [001] directions, respectively), characterizes a tilting of the oxygen octahedron centered around the Nb site  $i$  by  $0.1\sqrt{3}$  radians about the pseudocubic [111] direction.

The total energy of the  $H_{\text{eff}}$  of  $\text{NaNbO}_3$  is the sum of two main energies:

$$E^{\text{tot}} = E^{\text{FE}}(\{\mathbf{u}\}, \{\eta_l\}) + E^{\text{AFD}}(\{\mathbf{u}\}, \{\eta_l\}, \{\boldsymbol{\omega}\}), \quad (1)$$

where  $E^{\text{FE}}$  is the energy involving the local modes, elastic deformations, and their mutual couplings, while  $E^{\text{AFD}}$  includes the AFD motions and their interactions with strains and local modes.

$E^{\text{FE}}$  contains the following five terms, as proposed in Ref. [26]:

$$E^{\text{FE}} = E^{\text{self}}(\{\mathbf{u}\}) + E^{\text{dpl}}(\{\mathbf{u}\}) + E^{\text{short}}(\{\mathbf{u}\}) + E^{\text{elas}}(\{\eta_l\}) + E^{\text{int}}(\{\mathbf{u}\}, \{\eta_l\}), \quad (2)$$

where  $E^{\text{self}}$  is the local mode self energy,  $E^{\text{dpl}}$  is the long-range dipole-dipole interaction,  $E^{\text{short}}$  represents the short-range interactions between neighboring local modes excluding dipole-dipole interactions,  $E^{\text{elas}}$  is the elastic energy, and  $E^{\text{int}}$  is the interaction between elastic deformation and local modes. Explicitly, each term of  $E^{\text{FE}}$  reads:

$$\begin{aligned} E^{\text{self}} &= \sum_i \{ \kappa_2 u_i^2 + \alpha u_i^4 + \gamma (u_{ix}^2 u_{iy}^2 + u_{iy}^2 u_{iz}^2 + u_{ix}^2 u_{iz}^2) \} \\ E^{\text{dpl}} &= \frac{Z^{*2}}{\epsilon_\infty} \sum_{i < j} \frac{\mathbf{u}_i \cdot \mathbf{u}_j - 3(\hat{\mathbf{R}}_{ij} \cdot \mathbf{u}_i)(\hat{\mathbf{R}}_{ij} \cdot \mathbf{u}_j)}{R_{ij}^3} \\ E^{\text{short}} &= \sum_{i \neq j} \sum_{\alpha\beta} J_{ij\alpha\beta} u_{i\alpha} u_{j\beta} \\ E^{\text{elas}} &= \frac{N}{2} B_{11} (\eta_1^2 + \eta_2^2 + \eta_3^2) + N B_{12} (\eta_1 \eta_2 + \eta_2 \eta_3 + \eta_3 \eta_1) \\ &\quad + \frac{N}{2} B_{44} (\eta_4^2 + \eta_5^2 + \eta_6^2) \\ E^{\text{int}} &= \frac{1}{2} \sum_i \sum_{l\alpha\beta} B_{l\alpha\beta} \eta_l(\mathbf{R}_i) u_\alpha(\mathbf{R}_i) u_\beta(\mathbf{R}_i), \end{aligned} \quad (3)$$

where  $\mathbf{R}_{ij} = \mathbf{R}_i - \mathbf{R}_j$  with  $\mathbf{R}_i$  being the lattice vector of site  $i$ . The sums on  $i$  run over all Na sites, and  $\alpha$  and  $\beta$  are Cartesian components along the  $x$ ,  $y$ , and  $z$  axes. Moreover, the sum on  $j$  in  $E^{\text{dpl}}$  runs over all the Na sites that are different from  $i$ , while that on  $E^{\text{short}}$  runs over the first, second, and third nearest Na neighbors of the Na site  $i$ .

Furthermore, the interaction matrix  $J_{ij\alpha\beta}$  in  $E^{\text{short}}$  can be simplified for different nearest neighbor (NN) shells as:

$$\begin{aligned} \text{first NN: } J_{ij\alpha\beta} &= (j_1 + (j_2 - j_1)) \hat{\mathbf{R}}_{ij,\alpha} \delta_{\alpha\beta}; \\ \text{second NN: } J_{ij\alpha\beta} &= (j_4 + \sqrt{2}(j_3 - j_4)) \hat{\mathbf{R}}_{ij,\alpha} \delta_{\alpha\beta} \\ &\quad + 2j_5 \hat{\mathbf{R}}_{ij,\alpha} \cdot \hat{\mathbf{R}}_{ij,\beta} (1 - \delta_{\alpha\beta}); \\ \text{third NN: } J_{ij\alpha\beta} &= j_6 \delta_{\alpha\beta} + 3j_7 \hat{\mathbf{R}}_{ij,\alpha} \cdot \hat{\mathbf{R}}_{ij,\beta} (1 - \delta_{\alpha\beta}), \end{aligned} \quad (4)$$

TABLE I. Expansion parameters of the effective Hamiltonian for  $\text{NaNbO}_3$ . Atomic units are used here. The reference cubic lattice parameter is 7.388 Bohr.

Dipole	$Z^*$	8.8005	$\epsilon_\infty$	5.945		
$u$ on-site	$\kappa_2$	0.005112	$\alpha$	0.11975	$\gamma$	-0.22342
	$j_1$	-0.0101264	$j_2$	0.0335433		
$u$ short range	$j_3$	0.0036363	$j_4$	-0.0020866	$j_5$	0.0051405
	$j_6$	0.0005655	$j_7$	0.00028274		
Elastic	$B_{11}$	6.211	$B_{12}$	1.0818	$B_{44}$	1.032
$u\eta_l$ coup.	$B_{1xx}$	-1.4939	$B_{1yy}$	0.43861	$B_{4yz}$	-0.020843
$\omega$ on-site	$\kappa_A$	-0.073538	$\alpha_A$	2.69108	$\gamma_A$	-2.38182
$\omega$ short range	$k_1$	0.01838372	$k_2$	-0.000065656	$K'$	-0.0236641
$\omega\eta_l$ coup.	$C_{1xx}$	0.3093224	$C_{1yy}$	3.047636	$C_{4yz}$	-1.230160178
$\omega u$ coup. (trilinear)	$D_{ii,xy}$	-0.0139585				
$\omega u$ coup. (biquadratic)	$E_{xxxx}$	0.381915	$E_{xxyy}$	0.0968329	$E_{xyxy}$	-0.799544

where  $\hat{R}_{ij,\alpha}$  is the  $\alpha$  component of  $\mathbf{R}_{ij}/R_{ij}$  and  $\delta$  is the Kronecker symbol.

Moreover, the energy related to the oxygen octahedral tiltings and their couplings with the Na-centered  $\{u_i\}$  local modes and  $\eta_l$  strains is given by the expression provided in Ref. [44], that is:

$$\begin{aligned}
E^{\text{AFD}}(\{u_i\}, \{\eta_l\}, \{\omega_i\}) &= \sum_i [\kappa_A \omega_i^2 + \alpha_A \omega_i^4 + \gamma_A (\omega_{ix}^2 \omega_{iy}^2 + \omega_{iy}^2 \omega_{iz}^2 + \omega_{ix}^2 \omega_{iz}^2)] \\
&+ \sum_{ij} \sum_{\alpha\beta} K_{ij\alpha\beta} \omega_{i\alpha} \omega_{j\beta} \\
&+ \sum_i \sum_{\alpha} K' \omega_{i,\alpha}^3 (\omega_{i+\alpha,\alpha} + \omega_{i-\alpha,\alpha}) \\
&+ \sum_i \sum_{\alpha\beta} C_{i\alpha\beta} \eta_l(i) \omega_{i\alpha} \omega_{i\beta} \\
&+ \sum_{i,j} \sum_{\alpha,\beta} D_{ij,\alpha\beta} u_{j,\alpha} \omega_{i,\alpha} \omega_{i,\beta} \\
&+ \sum_{i,j} \sum_{\alpha\beta\gamma\delta} E_{\alpha\beta\gamma\delta} \omega_{i\alpha} \omega_{j\beta} u_{j\gamma} u_{i\delta}, \tag{5}
\end{aligned}$$

where the sums on  $i$  run over all the Nb sites, and  $\alpha$  and  $\beta$  are, once again, Cartesian components along the  $x$ ,  $y$ , and  $z$  axes coinciding with the pseudocubic [100], [010], and [001] directions, respectively. The first sum of  $E^{\text{AFD}}$  gathers the onsite contributions associated with the oxygen octahedral tiltings. It was proposed and/or used in Refs. [44–47]. The second and third terms characterize the short-range interactions between AFD motions, with  $j$  running over the Nb ions being first nearest neighbors of the Nb site  $i$ , and were given in Refs. [46] and [44], respectively. In this third term,  $\omega_{i+\alpha,\alpha}$  is the  $\alpha$  component of the AFD mode at the site shifted from the Nb site  $i$  to its nearest Nb neighbor along the  $\alpha$  axis. The fourth term of  $E^{\text{AFD}}$  describes the coupling between strain and AFD, as provided in Ref. [46]. The fifth and sixth terms of Eq. (5) comprise the coupling between AFD motions and local modes that include trilinear contributions (that are dependent on the  $D_{ij,\alpha\beta}$  coefficients) as well as biquadratic terms (that are quantified by the  $E_{\alpha\beta\gamma\delta}$  parameters). In these fifth and sixth terms,  $j$  runs over the eight Na atoms that are first nearest

neighbors of the Nb-site  $i$ . These fifth and sixth terms were introduced in Refs. [44] and [46], respectively.

Moreover, the  $K_{ij\alpha\beta}$  parameters entering the second energy of  $E^{\text{AFD}}$  can be simplified as:

$$\text{first NN: } K_{ij\alpha\beta} = (k_1 + (k_2 - k_1) |\hat{R}_{ij,\alpha}|) \delta_{\alpha\beta}. \tag{6}$$

All the parameters of Eqs. (3)–(6) are determined by performing several first-principle calculations on relatively small cells (typically, up to 40 atoms) using the local density approximation (LDA) [48] within density functional theory and the CUSP code [49] that takes advantage of the ultrasoft-pseudopotential scheme [50] (note that the same pseudopotentials as those given in Ref. [51] were used here, that is we consider the following valence electrons for Na ( $2s^2 2p^6 3s^1$ ), Nb ( $4s^2 4p^6 4d^4 5s^1$ ), and O ( $2s^2 2p^4$ ) ions, with a 25 Ry plane-wave cutoff). These parameters are listed in Table I, and we will often pay close attention to them in the following to understand but also revisit properties of  $\text{NaNbO}_3$ . Note that such parameters are extracted by considering small perturbations with respect to the cubic state and therefore do not rely on the full relaxation of any phase (see, e.g., Ref. [26] and references therein for more details on such extraction in the case of the coefficients entering  $E^{\text{FE}}$ ). As a result, the fact that we used LDA to obtain the parameters of  $H_{\text{eff}}$  of  $\text{NaNbO}_3$  does not automatically imply that our results for *relaxed* structures predicted by the effective Hamiltonian will be closer to those resulting from the direct use of LDA than to those of other functionals such as the generalized gradient approximation (GGA) in the form of revised Perdew-Burke-Ernzerhof [52] (PBEsol), especially if employing these two functionals within first-principles calculations provide similar results in terms of structure and minute differences between total energy of different relaxed phases—as it is, in fact, known in  $\text{NaNbO}_3$  bulk [53].

Once the different terms of the  $H_{\text{eff}}$  of  $\text{NaNbO}_3$  are identified and their parameters determined, we then employ this effective Hamiltonian within Monte-Carlo (MC) simulations on a  $12 \times 12 \times 12$  supercell (which corresponds to 8640 atoms). Note that we deliberately chose a length of 12 lattice constants along any Cartesian axis because this is the maximal periodicity ever reported for any phase in  $\text{NaNbO}_3$  bulk [12] and because

it is also commensurate with the periodicity of 4 and 6 lattice constants often suggested for some states of this system [13,54–56]. Such a choice therefore cannot lead to (presently unseen and unknown) phases for which the periodicity is not commensurate with 2, 3, 4, 6, or 12 lattice constants. For instance, a periodicity of, e.g., 16 lattice constants will not be captured by this choice. For each temperature, 40 000 MC sweeps are performed, with the first 20 000 allowing the system to equilibrate and the subsequent 20 000 being used to compute statistical averages.

### B. Direct first-principles calculations

We also conducted direct 0 K first-principles calculations, mostly to check the predictions of the aforementioned  $H_{\text{eff}}$  at low temperature but also to gain a deeper insight into  $\text{NaNbO}_3$ . For these latter calculations, we also used LDA [48] as well as GGA within the PBEsol functional [52], as implemented in the VASP package [57]. The projector augmented wave [57,58] (PAW) is applied to describe the core electrons. Seven electrons for Na ( $2p^63s^1$ ), 13 electrons for Nb ( $4s^24p^64d^45s^1$ ), and 6 electrons for O ions ( $2s^22p^4$ ) are treated as valence electrons. The plane-wave cutoff is set to be 550 eV. Different crystal structures (to be discussed below) within the perovskite lattice are fully relaxed until the Hellmann-Feynman force on each atom is converged to be less than 0.001 eV/Å. The transition path from one state to another was obtained using the variable-cell nudged elastic band method (VCNEB) [59] which is an extension of the nudged elastic band (NEB) technique included with the USPEX code [60–62] in combination with the VASP package. Phonon dispersion curves are calculated using the density functional perturbation theory (DFPT), as implemented in the ABINIT package [63–65]. Exchange and correlation functional is treated with optimized norm-conserving pseudopotentials [66], with the Perdew-Burke-Ernzerhof (PBE) parametrization. The wave functions are expanded using plane-wave basis sets with a kinetic energy cutoff of 30 Hartree. The self-consistent calculations are performed with an unshifted  $4 \times 4 \times 2$   $k$ -point grid. The same grid is used for  $q$  point in the phonon calculation.

## III. RESULTS

### A. Results at small temperature

Running simulations at low temperature (namely, 10 K) within the effective Hamiltonian described above, along with its parameters given in Table I, provide a  $R3c$  ground state, as consistent with measurements [21,67]. Such an  $R3c$  state is characterized by a polarization lying along the pseudocubic [111] direction altogether with oxygen octahedra tilting in antiphase about this polarization axis (its oxygen tilting pattern is thus described by  $a^-a^-a^-$  in Glazer notation [68]). Table II provides the total energy (with respect to the equilibrium paraelectric  $Pm\bar{3}m$  phase) of this  $R3c$  state, as well as that of two specific other states that the effective Hamiltonian predicts to be of rather low energy, namely a  $Pnma$  state and a state that we will refer to here as Phase 1.

The  $Pnma$  state is one of the most common phases of perovskites and possesses three main finite order parameters

TABLE II. Internal energies, in meV per 5 atoms, of the  $R3c$ ,  $Pnma$ , and Phase 1/ $Pca2_1$  states of  $\text{NaNbO}_3$  at 10 K, as predicted from the presently developed  $H_{\text{eff}}$ , LDA, and PBEsol simulations. The zero of energy corresponds to the equilibrium cubic paraelectric  $Pm\bar{3}m$  state.

State	$H_{\text{eff}}$	LDA	PBEsol
$R3c$	−155.93	−199.69	−108.70
$Pnma$	−150.24	−198.61	−91.66
Phase 1/ $Pca2_1$	−155.53	−201.41	−107.46

[69]: (1) an antiphase tilting of the oxygen octahedra about the pseudocubic [110] direction (such tilting is associated with the  $R$  point of the cubic first Brillouin zone); (2) an in-phase tilting of the oxygen octahedra about the pseudocubic [001] direction (the corresponding  $k$  point is the  $M$  point of the cubic first Brillouin zone)—therefore yielding the  $a^-a^-c^+$  Glazer notation [68] for the whole tilting pattern; and (3) an antipolar vector corresponding to displacements of Na ions being along the pseudocubic [110] direction in one of every other (001) planes and along the opposite  $[\bar{1}\bar{1}0]$  direction in the other subsequent (001) planes (this antipolar vector is therefore associated with the  $X$  point of the cubic first Brillouin zone). These three order parameters are coupled via a trilinear coupling whose strength is related to the  $D_{ii,xy}$  coefficient of Table I, as demonstrated in Ref. [70].

Phase 1 is, to the best of our knowledge, a phase that has been overlooked in  $\text{NaNbO}_3$ . It has a spontaneous polarization along the pseudocubic [001] axis but which is not fully homogeneous. For instance, doing a Fourier transform of the  $z$  component of the local dipoles [71] in our  $12 \times 12 \times 12$  supercell leads to a 88% weight on the  $\Gamma$  point (which is associated with the polarization) but also to an additional 10% on the  $X$  point (which corresponds to antipolar motions along the [001] axis) at 10 K. Furthermore, Phase 1 also exhibits antiphase tilting of the oxygen octahedra about the pseudocubic [110] direction. It further possesses a complex oxygen octahedral tilting about the [001] direction that is associated with the reciprocal  $k$  point lying halfway between the  $M$  and  $R$  points. As a result, a periodic series of “++−−” occur for the tilting pattern about the  $z$  axis when moving along any [001] line, implying that Phase 1 is a *nanotwin* or a long-period modulated state [44,72] having a periodicity of four lattice constants. Antipolar displacements of the Na ions along [110] and that are indexed by the  $k$  point being halfway between the  $\Gamma$  and  $X$  points also emerge in this Phase 1, because of a trilinear coupling (also involving the  $D_{ii,xy}$  coefficient of Table I) between these antipolar displacements, the antiphase oxygen octahedral tiltings about the [110] direction, and the more complex tilting pattern about the [001] direction [70]. The periodic pattern of the  $x$  and  $y$  components of these antipolar displacements is of the type “+0−0” when moving along the  $z$  axis. All these polar, antipolar, and tilting pattern features likely imply that Phase 1 adopts the  $Pca2_1$  space group. It is interesting to realize that (i)  $Pca2_1$  can be thought of as being derived from the  $Pbcm$  state (that is well known in pure  $\text{NaNbO}_3$  [54,73]), but when superposing a spontaneous (inhomogeneous) polarization along the [001] axis and (ii) that a  $Pca2_1$

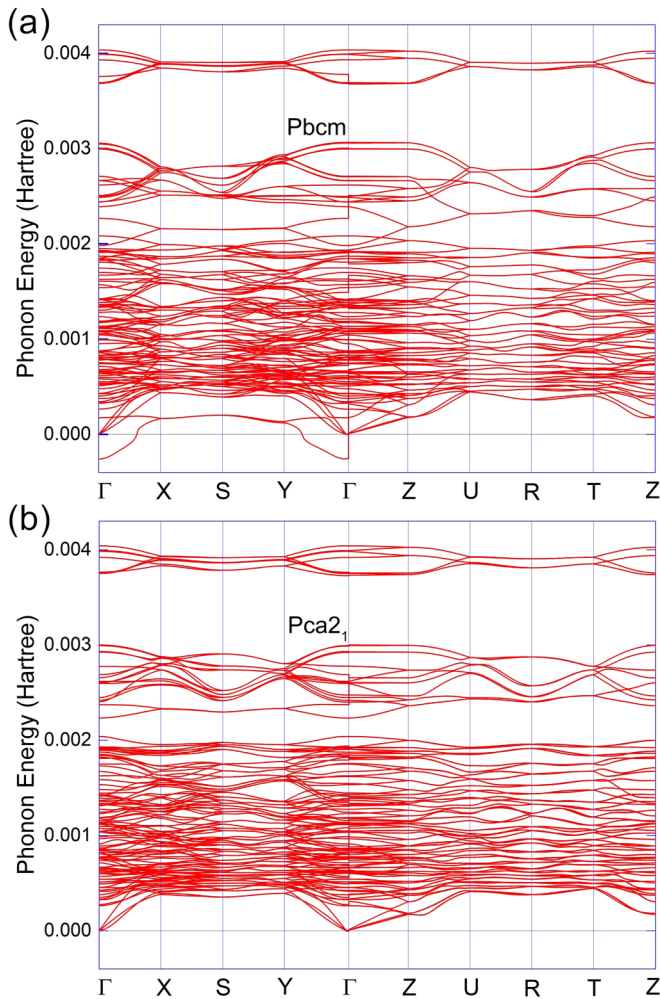


FIG. 1. Phonon spectrum of the *Pbcm* (a) and *Pca2<sub>1</sub>* (b) states, as predicted by the direct use of first-principle DFPT calculations. Notice the unstable modes (having negative frequencies) around  $\Gamma$  for the *Pbcm* state.

phase has been reported near room temperature when slightly doping  $\text{NaNbO}_3$  by Li such as to make the  $(\text{Li}_{0.02}\text{Na}_{0.98})\text{NbO}_3$  compound [54]. Furthermore, we numerically find that starting the  $H_{\text{eff}}$  simulations with a pure *Pbcm* state at low temperatures results in the formation of Phase 1 after relaxation, mostly because of the large negative value of the  $E_{xyxy}$  coefficient of Table I—which favors a coupling between the out-of-plane polarization, in-plane antipolar displacements, antiphase tiltings, and the more complex tilting pattern about the [001] direction. Interestingly, direct 0 K first-principles calculations predict that (1) the phonon spectrum of *Pbcm* exhibits unstable modes (especially around the  $\Gamma$  zone center), unlike that of *Pca2<sub>1</sub>*, as depicted in Fig. 1, and (2) *Pca2<sub>1</sub>* has a lower energy than *Pbcm* by 0.12 meV per 5 atoms (when using the PBEsol functional). Items (1) and (2) therefore further strongly suggest the possibility of finding Phase 1/*Pca2<sub>1</sub>* rather than *Pbcm* in  $\text{NaNbO}_3$  at low temperature. The polarization of Phase 1 is predicted to be about 0.18 C/m<sup>2</sup> at 10 K by our effective Hamiltonian, which is about 2.5 smaller than the predicted polarization of the *R3c* state by the  $H_{\text{eff}}$  method (note that this smaller value of the polarization of Phase 1 may explain

the previous overlooking of this state at low temperatures, especially in samples for which coexistence of phases with the *R3c* state are known to occur [22]). Interestingly, the direct use of first-principles calculations using the PBEsol functional provides a polarization of the order of 0.13 C/m<sup>2</sup> for *Pca2<sub>1</sub>*, which indicates that our current effective Hamiltonian yields the right order of magnitude of the spontaneous polarization of Phase 1. (Note that our fully *ab initio* calculations within LDA functional basically gives the same energy for *Pbcm* and *Pca2<sub>1</sub>* and yields a smaller polarization of 0.05 C/m<sup>2</sup> for the *Pca2<sub>1</sub>* state. However, the LDA functional is also previously known to wrongly predict that *Pbcm* has a lower internal energy than *R3c* in  $\text{NaNbO}_3$  [53]—therefore casting some doubts about direct 0 K LDA results for some relaxed states.)

Moreover, Table II indicates that the effective Hamiltonian with the parameters listed in Table I yields internal energies for *R3c*, *Pnma*, and Phase 1/*Pca2<sub>1</sub>* that are basically all halfway between those of our direct LDA and PBEsol calculations. It also reveals that the energies of *R3c* and Phase 1/*Pca2<sub>1</sub>* are very close to each other (namely, within 2 meV/5 atom), while that of *Pnma* is further away but by less than 17 meV per 5 atom, in all types of calculations. It is also interesting to notice that the direct LDA calculations incorrectly predict that *Pca2<sub>1</sub>* is the ground state of  $\text{NaNbO}_3$ , which contradicts experimental results but which is consistent with previous LDA computations indicating that *Pbcm* has a lower energy than *R3c* [53]. On the other hand, both the  $H_{\text{eff}}$  and PBEsol calculations correctly give a *R3c* ground state, with the (negative) difference in energy between *R3c* and Phase 1 arising from the effective Hamiltonian being about  $-0.4$  meV per 5 atom—which is therefore (once again) in between the positive difference in energy between *R3c* and *Pca2<sub>1</sub>* of  $+1.7$  meV per 5 atom given by LDA simulations and the corresponding negative difference in energy of  $-1.2$  meV per 5 atom provided by the PBEsol computations.

Furthermore, Figs. 2(a) and 2(b) reveal that the hierarchy between the  $H_{\text{eff}}$  energies of these three phases can be dramatically altered by varying the  $E_{xyxy}$  and  $D_{ii,xy}$  coefficients, respectively, therefore demonstrating the crucial importance of coupling between cation displacements and oxygen octahedral tiltings in  $\text{NaNbO}_3$ . More precisely, making the  $E_{xyxy}$  parameter less negative with respect to its value given in Table I first results in Phase 1 and then *Pnma* becoming the states of lowest energy [see Fig. 2(a)]—which indicates that having a large and negative  $E_{xyxy}$  coefficient is essential to make *R3c* the (experimental) ground state of  $\text{NaNbO}_3$ . Such evolution from *R3c* to *Pnma*, via Phase 1, can also be accomplished by making the  $D_{ii,xy}$  trilinear coupling parameter more negative, as shown in Fig. 2(b), since the energy of *Pnma* is rather sensitive to it, unlike that of *R3c*, while that of Phase 1 also depends on  $D_{ii,xy}$  but to a smaller extent than *Pnma*—as consistent with the energetic term of Eq. (5) involving  $D_{ii,xy}$  (and that is provided and analyzed in detail in Ref. [70]). Interestingly, Fig. 2 can also be thought of as indicating that a small uncertainty in the determination of the  $E_{xyxy}$  and  $D_{ii,xy}$  coefficients can lead to a change in ground state, which may further explain why our effective Hamiltonian method (with its LDA-determined coefficients) yields a *R3c* ground state, unlike fully relaxed direct LDA calculations.

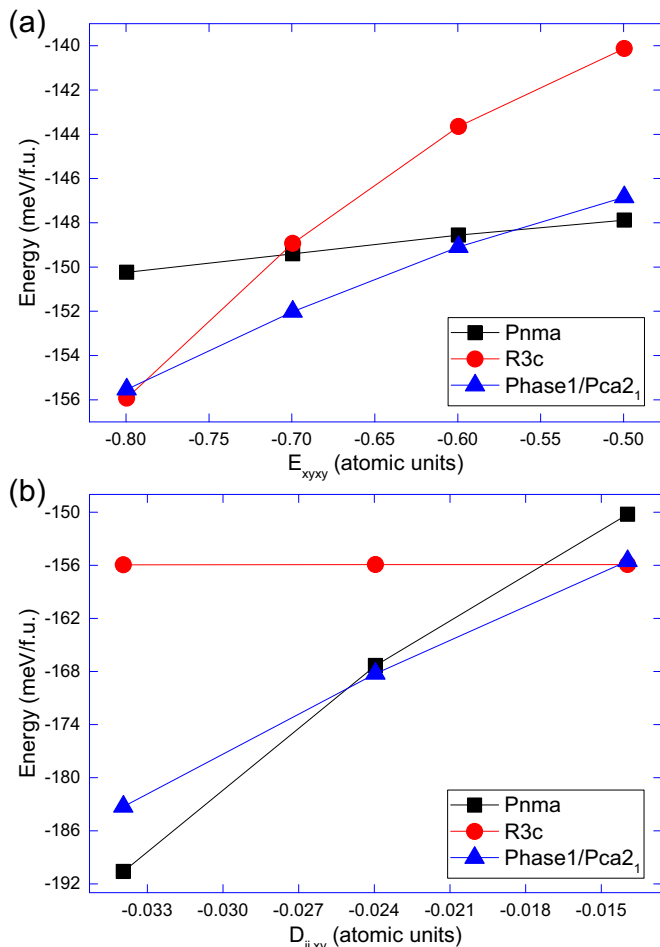


FIG. 2. Dependency of the  $H_{\text{eff}}$  internal energy of the  $R3c$ ,  $Pnma$ , and Phase 1/ $Pca2_1$  phases at 10 K, as a function of the  $E_{xyxy}$  (a) and  $D_{ii,xy}$  (b) coefficients. The other effective Hamiltonian parameters are those given in Table I during these two variations and energies are given in meV per 5 atom, with the zero in energy referring to the equilibrium cubic paraelectric  $Pm\bar{3}m$  state (i.e., having a lattice parameter of 7.388 Bohr).

### B. Results as a function of temperature

The temperature behavior of  $\text{NaNbO}_3$  is experimentally known to be extraordinarily complex since it involves several phases, including some being under intense discussion—as evidenced by the facts that different experimental groups proposed different space groups for, e.g., the  $R$  and  $S$  phases [12,13,55,74] and even suggested that the  $P$  state can consist of three different phases [75]. Such complexity is encountered in our Monte-Carlo simulations using the effective Hamiltonian. For instance, if we cool the system from high to low temperatures, the  $H_{\text{eff}}$  calculations provide a  $Pnma$  state for the lowest temperatures, despite the fact that the energy of  $R3c$  is lower than that of  $Pnma$  by more than 5 meV per 5 atom (see Table II). Similarly, if we start from the  $R3c$  ground state and heat up  $\text{NaNbO}_3$  bulk, neither  $Pbcm$  state nor  $Pbcm$ -like phases (such as Phase 1/ $Pca2_1$ ) emerge in the simulations up to the highest investigated temperatures, at which the system is paraelectric cubic, while such latter phases are well known to exist in the phase diagram of pure and slightly-doped

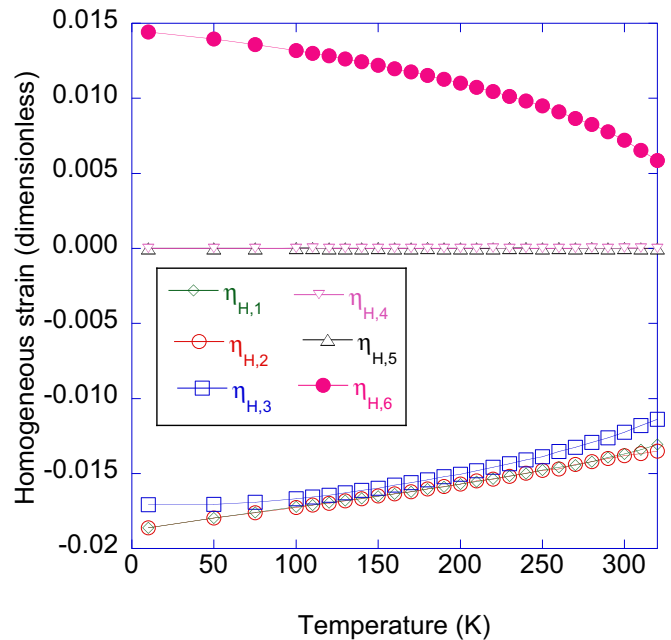


FIG. 3. Temperature dependency of the components of the homogeneous strain tensor between 10 and 320 K, as predicted by the presently developed effective Hamiltonian. The zero of strain corresponds to the equilibrium cubic paraelectric  $Pm\bar{3}m$  state (i.e., having a lattice parameter of 7.388 Bohr). The error bars on the finite elements of the strain tensor range between  $5.5$  and  $8.3 \times 10^{-4}$  at 300 K, that is at least one order of magnitude smaller than the average values of such strain elements.

$\text{NaNbO}_3$  compounds [14,54,56]. Such difficulties arise from the facts that several and rather crystallographically-different phases have very close free energies in  $\text{NaNbO}_3$  and that the barrier between such phases is rather high. For instance, we numerically found (not shown here) that the energetic barrier between  $R3c$  to  $Pca2_1$  is as large as 14 meV/5 atom when using the PBEsol functional within direct *ab initio* calculations, with this barrier being associated with a state of  $Pc$  symmetry—while  $R3c$  and  $Pca2_1$  have very similar internal energy, as indicated in Table II.

As a result, we adopt the following strategy here: We start our MC calculations with the aforementioned Phase 1 at 10 K and progressively heat up the system until it transforms into the  $Pm\bar{3}m$  paraelectric cubic state. We extract the following quantities from the outputs of the MC simulations at any investigated temperature: (1) all six components of the homogeneous strain tensor; (2) the  $\langle \mathbf{u} \rangle$  supercell average of the local mode vectors  $\{\mathbf{u}_i\}$ , which is directly proportional to the spontaneous electric polarization; (3) the  $\langle \omega_{\mathbf{R}} \rangle$  vector that characterizes *antiphase* tilting of the oxygen octahedra [43] and that is defined as  $\omega_{\mathbf{R}} = \frac{1}{N} \sum_i \omega_i (-1)^{n_x(i)+n_y(i)+n_z(i)}$ , where the sum runs over the  $N$  sites  $i$  and  $n_x(i)$ ,  $n_y(i)$  and  $n_z(i)$  are integers locating the cell  $i$  [in the ideal perovskite structure, and denoting the 5-atom cubic lattice constant by  $a_{\text{lat}}$ , this cell  $i$  is centered at  $a_{\text{lat}}(n_x(i)\mathbf{x} + n_y(i)\mathbf{y} + n_z(i)\mathbf{z})$ ]; and (4) the  $\langle \omega_{\mathbf{M}_x} \rangle$ ,  $\langle \omega_{\mathbf{M}_y} \rangle$ , and  $\langle \omega_{\mathbf{M}_z} \rangle$  vectors that represent *in-phase* oxygen octahedral tiltings and that are given by  $\omega_{\mathbf{M}_x} = \frac{1}{N} \sum_i \omega_i (-1)^{n_y(i)+n_z(i)}$ ,  $\omega_{\mathbf{M}_y} = \frac{1}{N} \sum_i \omega_i (-1)^{n_x(i)+n_z(i)}$ ,

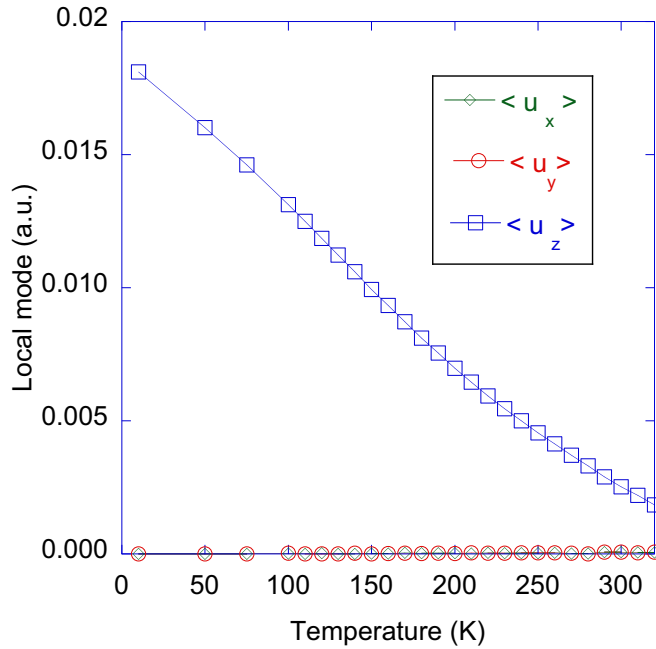


FIG. 4. Temperature dependency of the supercell average of the local mode vectors between 10 and 320 K, as predicted by the presently developed effective Hamiltonian. The error bar on  $\langle u_z \rangle$  is equal to  $6 \times 10^{-4}$  at 300 K, that is about one order of magnitude smaller than  $\langle u_z \rangle$ .

and  $\omega_{\mathbf{M}_z} = \frac{1}{N} \sum_i \omega_i (-1)^{n_x(i) + n_y(i)}$ . The strain,  $\langle \mathbf{u} \rangle$  and  $\langle \omega_{\mathbf{R}} \rangle$  are shown in Figs. 3, 4, and 5, respectively, as a function of temperature up to 320 K (no in-phase tiltings are found up to 320 K, which explains why we do not display  $\langle \omega_{\mathbf{M}_x} \rangle$ ,  $\langle \omega_{\mathbf{M}_y} \rangle$ , or  $\langle \omega_{\mathbf{M}_z} \rangle$  in this temperature range). They are also depicted in Figs. 6, 7, and 8, respectively, but within the smaller temperature window ranging between 320 K and 390 K, because, as we will see below, various phase transitions are predicted there. Note that Fig. 9 further reports the  $y$  component of  $\langle \omega_{\mathbf{M}_y} \rangle$  in this smaller interval because it is the only component out of those of all in-phase pseudovectors that is numerically found to be finite for some temperatures there. We also performed Fourier transform of the last MC configuration of both the local modes and tilting patterns [71] at any temperature, in order to identify possible significant  $k$  points that are associated with the phases presently numerically found and to be discussed below. Note that such phases can be complex, implying that some of these  $k$  points are neither at the zone center nor at the zone boundary of the cubic first Brillouin zone. For instance, in our aforementioned Phase 1/ $Pca2_1$  state, such  $k$  points are  $\frac{2\pi}{4a_{\text{lat}}} \mathbf{z}$  for the pattern of the  $x$  and  $y$  components of the  $\mathbf{u}_i$  local modes and  $\frac{2\pi}{a_{\text{lat}}} (\frac{1}{2} \mathbf{x} + \frac{1}{2} \mathbf{y} + \frac{1}{4} \mathbf{z})$  for the configuration of the  $z$  component of the  $\omega_i$  AFD pseudovectors. All significant  $k$  points are reported in Table III for the phases that the MC simulations numerically found and that we are going to discuss in details below. We adopt here the convention that  $\mathbf{k}_{\mathbf{u},x}$ ,  $\mathbf{k}_{\mathbf{u},y}$ ,  $\mathbf{k}_{\mathbf{u},z}$  correspond to the significant  $k$  point(s) found in the Fourier transform of the configuration of the  $x$ ,  $y$ , and  $z$  components of the local modes, respectively. Similarly,  $\mathbf{k}_{\text{AFD},x}$ ,  $\mathbf{k}_{\text{AFD},y}$ , and  $\mathbf{k}_{\text{AFD},z}$  are the  $k$  points having significant weights in the Fourier transform of the pattern of the  $x$ ,  $y$ , and  $z$  components of the

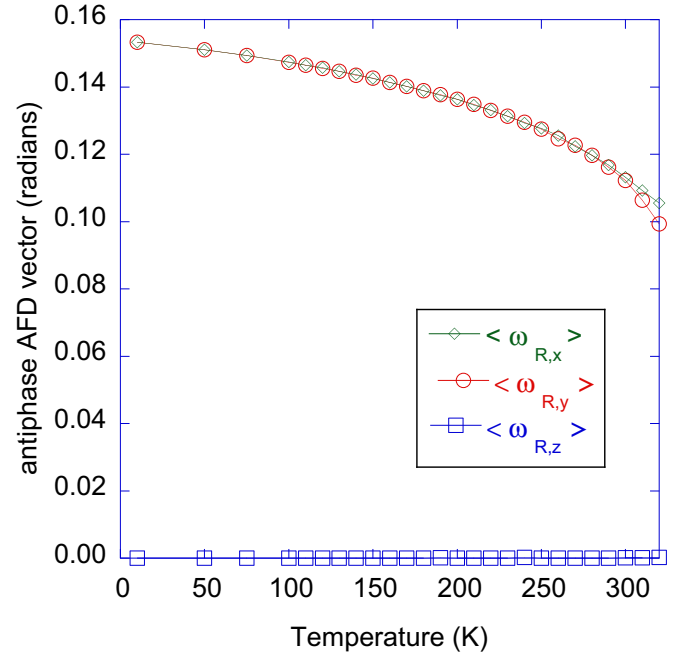


FIG. 5. Temperature dependency of the  $\langle \omega_{\mathbf{R}} \rangle$  antiphase tilting vector between 10 and 320 K, as predicted by the presently developed effective Hamiltonian. The error bars on  $\langle \omega_{R,x} \rangle$  and  $\langle \omega_{R,y} \rangle$  are about  $5 \times 10^{-3}$  at 300 K, that is about two orders of magnitude smaller than  $\langle \omega_{R,x} \rangle$  and  $\langle \omega_{R,y} \rangle$ .

$\omega_i$  AFD pseudovectors, respectively. In some cases, several  $k$  points occur for the same pattern, some of them having a major weight while others are minor, but all the  $k$  points having a weight larger than 5% are reported in Table III. Note that we can not practically determine the space group of the phases to be discussed below, mostly due to the significant fluctuations experienced by the tiltings between the different sites of the supercells at finite temperature as well as because of the large supercell used in our simulations. We nevertheless hope that all the structural information we are providing below can be useful to experimentalists when trying to fit their data by some specific space groups.

Figures 3, 4, and 5 indicate that  $\text{NaNbO}_3$  bulk is predicted to stay within Phase 1 at least up to 320 K, with the degrees of freedom of this phase decreasing in magnitude when the temperature increases. For instance and as seen in Fig. 4, the  $z$  component of  $\langle \mathbf{u} \rangle$  (which is directly related to the out-of-plane polarization of Phase 1) decreases from 0.0181 atomic units at 10 K to a value as small as 0.0025 atomic units at 300 K, which corresponds to a rather small polarization of  $\simeq 0.02$  C/m<sup>2</sup> and which may thus explain why Phase 1 has been overlooked in favor of  $Pbcm$  in previous measurements of the  $P$  phase of  $\text{NaNbO}_3$  [12,56] (recall that  $Pbcm$  has no polarization). Similarly and as indicated in Fig. 5, the antiphase tilting about the [110] pseudocubic is reduced as the temperature increases up to 320 K. The negative  $\eta_{H,1} = \eta_{H,2}$  elements of the homogeneous strain tensor, as well as the slightly less negative  $\eta_{H,3}$  and the shear strain  $\eta_{H,6}$ , also all get reduced in magnitude during that heating within Phase 1, as displayed in Fig. 3. Note that such strain tensor is indicative of an

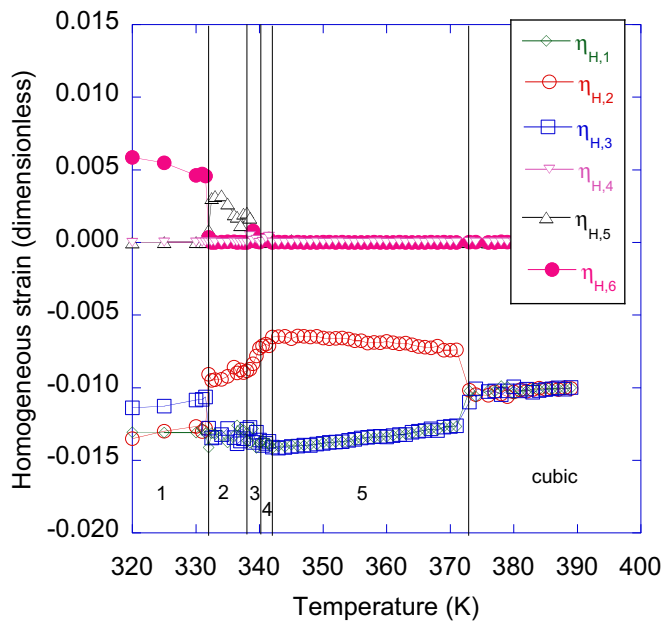


FIG. 6. Temperature dependency of the components of the homogeneous strain tensor between 320 and 390 K, as predicted by the presently developed effective Hamiltonian. The zero of strain corresponds to the equilibrium cubic paraelectric  $Pm\bar{3}m$  state (i.e., having a lattice parameter of 7.388 Bohr). The vertical solid lines depict transition temperatures, and the ‘1,’ ‘2,’ ‘3,’ ‘4,’ ‘5,’ and ‘cubic’ notations refer to the Phases 1, 2, 3, 4, and 5, as well as the paraelectric cubic state, discussed in the text. The same vertical scale is used as in Fig. 3, for comparison. The error bars on the diagonal elements of the strain tensor are about  $7 \times 10^{-4}$  at 335 K, that is at least one order of magnitude smaller than the average values of such strain elements. The error bar on  $\eta_{H,5}$  is about  $10^{-3}$  at 335 K, which is about three times smaller than the average value of this shear strain component.

orthorhombic symmetry for Phase 1, as consistent with a  $Pca2_1$  space group.

On the other hand, Figures 6–9, along with Table III, are full of new information (note, in particular, that Table III is going to be rather useful to analyze tilting patterns, especially because Fig. 8 demonstrates that  $\langle \omega_{\mathbf{R}} \rangle$  experiences rather large fluctuations, likely because several phases have similar free energies). For instance, at about 332 K, a transition from Phase 1 to a state coined here as Phase 2 is happening in the MC simulations. Phase 2 is characterized by  $\eta_{H,2}$  being now the smallest-in magnitude (but still negative) diagonal element of the strain tensor, while the (negative too)  $\eta_{H,3}$  becomes now equal to  $\eta_{H,1}$  and the only nonzero shear strain is now  $\eta_{H,5}$ . Such change in strain is linked to modifications of the tilting patterns: The antiphase tiltings are now about both the  $x$  and  $z$  axes, with these two tiltings being not necessarily equal to each other anymore in magnitude (see Fig. 8), while the tilting about the  $y$  axis has now the  $\frac{2\pi}{a_{\text{lat}}}(\frac{1}{2}, \frac{1}{6}, \frac{1}{2})$   $k$  point as its majority  $k$  point. However, Table III further informs us that two other  $k$  points, namely  $\frac{2\pi}{a_{\text{lat}}}(\frac{1}{2}, \frac{1}{4}, \frac{1}{2})$  and the  $M$  point, are also involved to a lesser extent in the oxygen octahedral pattern about the  $y$  axis in Phase 2 (note that the occurrence of this  $M$  point is fully consistent with the small but finite and nearly constant value of  $\langle \omega_{\mathbf{M}_y} \rangle$  shown in Fig. 9 between 332 K and 338 K). The

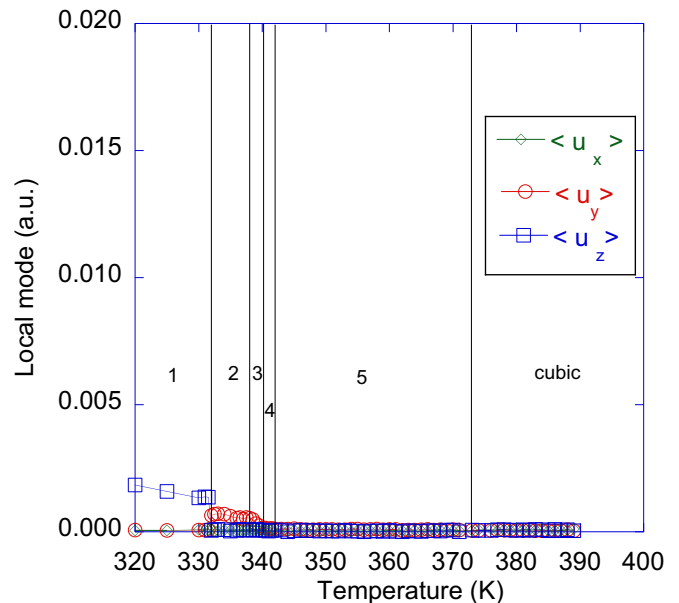


FIG. 7. Temperature dependency of the supercell average of the local mode vectors between 320 and 390 K, as predicted by the presently developed effective Hamiltonian. The vertical solid lines depict transition temperatures, and the ‘1,’ ‘2,’ ‘3,’ ‘4,’ ‘5,’ and ‘cubic’ notations refer to the Phases 1, 2, 3, 4, and 5, as well as the paraelectric cubic state, discussed in the text. The same vertical scale is used as in Fig. 4, for comparison. The error bar on  $\langle u_y \rangle$  is equal to  $6 \times 10^{-4}$  at 335 K, which is of the same order as  $\langle u_y \rangle$  itself, implying that  $\langle u_y \rangle$  is statistically null—as consistent with the ‘N/A’ wording used for  $\mathbf{k}_{\mathbf{u}_y}$  in Table III.

resulting pattern of oxygen octahedral tilting about the  $y$  axis is found to be of the periodic form “---++++---++++” when moving along any [010] line. Phase 2 is therefore also a nanotwin phase [44] but now having a periodicity of twelve lattice constants along the  $y$  direction. One can then propose to characterize such a tilting pattern by extending the Glazer notation as  $a^-b^{\text{complex}}.12c^-$  to indicate that the  $x$ - and  $z$ -axis experience antiphase tiltings that are not necessarily of the same magnitude while there is a complex tilting of 12-lattice constant periodicity about the  $y$  axis in Phase 2. Note that in that extension of the Glazer notations, the tilting pattern of Phase 1 (which is our  $P$  phase) is described as  $a^-a^-c^{\text{complex}.4}$  and that we will use such extended notations to characterize other phases to be discussed soon. On the other hand, no overall long-range polar or antipolar cation motions occur in Phase 2, as evidenced by the “N/A” wording ascribed to  $\mathbf{k}_{\mathbf{u}_x}$ ,  $\mathbf{k}_{\mathbf{u}_y}$ ,  $\mathbf{k}_{\mathbf{u}_z}$  in Table III. We propose that Phase 2 is the  $R$  state of  $\text{NaNbO}_3$ , especially since its majority  $k$  point is  $\frac{2\pi}{a_{\text{lat}}}(\frac{1}{2}, \frac{1}{6}, \frac{1}{2})$  and thus will imply a periodicity of six lattice constants (when taken alone), as indeed proposed in Refs. [12,55,74]. Note that it is the additional  $\frac{2\pi}{a_{\text{lat}}}(\frac{1}{2}, \frac{1}{4}, \frac{1}{2})$  of Table III that, altogether with  $\frac{2\pi}{a_{\text{lat}}}(\frac{1}{2}, \frac{1}{6}, \frac{1}{2})$ , makes our Phase 2 adopting a periodicity of 12 rather than 6 lattice constants along its long axis. It is also important to realize that the  $P$ -to- $R$  transition has been observed to be of first order [12], which is also in line with the predicted jump of some strain components at about 332 K in our Fig. 6.

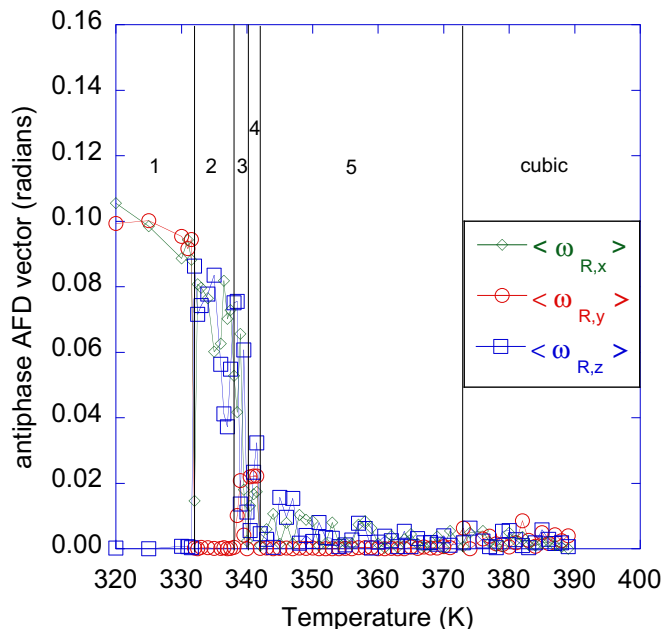


FIG. 8. Temperature dependency of the  $\langle \omega_{\mathbf{R}} \rangle$  antiphase tilting vector between 320 and 390 K, as predicted by the presently developed effective Hamiltonian. The vertical solid lines depict transition temperatures, and the ‘1,’ ‘2,’ ‘3,’ ‘4,’ ‘5,’ and ‘cubic’ notations refer to the Phases 1, 2, 3, 4, and 5, as well as the paraelectric cubic state, discussed in the text. The same vertical scale is used as in Fig. 5, for comparison. The error bars on  $\langle \omega_{R,x} \rangle$  and  $\langle \omega_{R,z} \rangle$  range between 1 and  $2 \times 10^{-2}$  at 335 K, that is about three to four times smaller than  $\langle \omega_{R,x} \rangle$  and  $\langle \omega_{R,z} \rangle$ .

Moreover, Phase 2 is found to persist up to 338 K, at which point it makes way to a state that we denote as Phase 3 and that remains stable until 340 K. Some changes between Phases 2 and 3 are rather subtle, in the sense that (i) all three significant  $k$  points characterizing the tilting pattern about the  $y$  axis of Phase 2 are still there in Phase 3 but with the difference that the majority point is now the  $M$  point, as evidenced by the sudden increase of  $\langle \omega_{M,y} \rangle$  when increasing the temperature from 338 K to 341 K, as shown in Fig. 9, and (ii) an additional  $k$  point emerges in such a tilting pattern, that is  $\frac{2\pi}{a_{\text{lat}}}(\frac{1}{2}, \frac{1}{12}, \frac{1}{2})$ , therefore further emphasizing an overall periodicity along the  $y$  axis of 12 lattice constants. Note that the tilting pattern of Phase 3 about the  $y$  axis varies from that of Phase 2, via the formation of the “- - + + + + + + - + + +” periodic series along any [010] line, that is by replacing the - sign in the eighth site of the tilting sequence in Phase 2 by an opposite sign in Phase 3. Phase 3 differs also from Phase 2 by the vanishing of antiphase tiltings about the  $x$  axis, unlike for the  $z$  axis. In other words, Phase 3 is still a nanotwin state (likely of orthorhombic or monoclinic symmetry, according to the finite strain elements depicted in Fig. 6) but with a description being of the form  $a^0 b^{\text{complex}, 12} c^-$ . Such a Phase 3 is presently suggested to be the documented  $S$  state of  $\text{NaNbO}_3$ , which has also been reported to have a 12-lattice constant periodicity along a pseudocubic  $\langle 100 \rangle$  axis [12] (note that the longer periodicity is along the  $y$  axis in our case while it is about the  $z$  axis in Ref. [12], but such axes are symmetrically equivalent—that is, we can also find in our simulations a Phase 3 for which

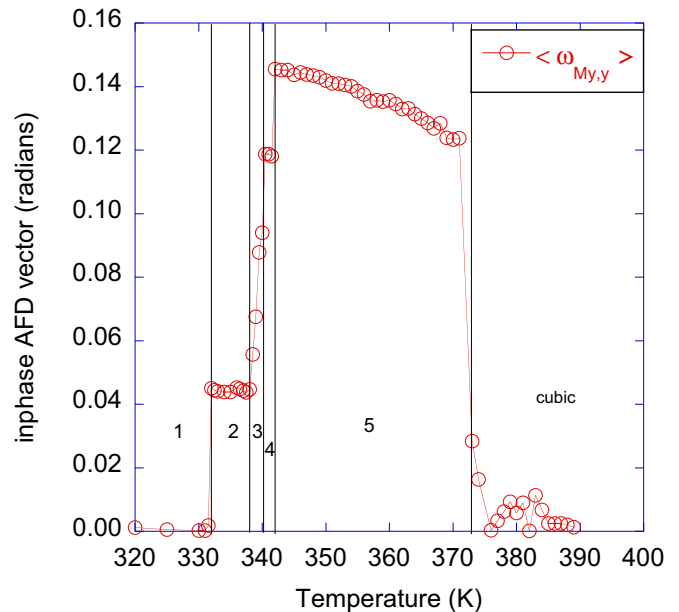


FIG. 9. Temperature dependency of the  $y$  component of the  $\langle \omega_{M_y} \rangle$  in-phase tilting pseudovector between 320 and 390 K, as predicted by the presently developed effective Hamiltonian. The vertical solid lines depict transition temperatures, and the ‘1,’ ‘2,’ ‘3,’ ‘4,’ ‘5,’ and ‘cubic’ notations refer to the Phases 1, 2, 3, 4, and 5, as well as the paraelectric cubic state, discussed in the text. The same vertical scale is used as in Figs. 5 and 8, for comparison. The error bar on  $\langle \omega_{M_y,y} \rangle$  is about  $10^{-2}$  at 370 K, that is about one order of magnitude smaller than  $\langle \omega_{M_y,y} \rangle$ .

the longer axis is along the pseudocubic [001] direction). It is also interesting to realize that Refs. [13,55] rather proposed that the  $S$  structure is of the type  $a^- b^+ c^+$ ,  $a^+ b^+ c^{\text{complex}, 4}$  or  $a^0 b^+ c^{\text{complex}, 4}$ , that is either having an in-phase tilting or a complex tilting of four-lattice constant periodicity about the  $z$  axis and that such tiltings are in fact related to  $k$  points appearing in Table III for Phase 3 too when interchanging the  $y$  and  $z$  axes [i.e.,  $\frac{2\pi}{a_{\text{lat}}}(\frac{1}{2}, \frac{1}{2}, 0)$  and  $\frac{2\pi}{a_{\text{lat}}}(\frac{1}{2}, \frac{1}{2}, \frac{1}{4})$ ]. However, as indicated above, the overall periodicity about the long axis of Phase 3 is presently found to be of 12 lattice constants because of the presence of the minority  $\frac{2\pi}{a_{\text{lat}}}(\frac{1}{2}, \frac{1}{12}, \frac{1}{2})$   $k$  point, as well as the existence of  $\frac{2\pi}{a_{\text{lat}}}(\frac{1}{2}, \frac{1}{6}, \frac{1}{2})$  in addition to  $\frac{2\pi}{a_{\text{lat}}}(\frac{1}{2}, \frac{1}{4}, \frac{1}{2})$ . The fact that  $\frac{2\pi}{a_{\text{lat}}}(\frac{1}{2}, \frac{1}{12}, \frac{1}{2})$  and  $\frac{2\pi}{a_{\text{lat}}}(\frac{1}{2}, \frac{1}{6}, \frac{1}{2})$  are of minority rather than of majority may explain why Refs. [13,55] did not report an overall periodicity of 12 lattice constants for the  $S$  state.

A phase, termed as Phase 4, emerges at about 340 K and is stable up to 342 K. Phase 4 differs from Phase 3 by the occurrence of “only” in-phase tiltings about the  $y$  axis. In other words, Phase 4 is not a nanotwin anymore but is rather a state that is described by the conventional Glazer notation [68] as  $a^0 b^+ c^-$ . Such a simpler state is consistent with the  $a^- b^0 c^+$  phase proposed for the so-called  $T_1$  phase of  $\text{NaNbO}_3$  [13], which is orthorhombic and of  $C_{\text{cmm}}$  space group. Note that the new tilting pattern of Phase 4 with respect to Phase 3 leads to the stabilization of  $\langle \omega_{M_y} \rangle$  to a fixed value (see Fig. 9).

TABLE III. Significant  $k$  points associated with the phases numerically found by the MC simulations using the presently developed effective Hamiltonian, in  $\frac{2\pi}{a_{\text{lat}}}$  unit. The wordings “maj” and “min” refer to  $k$  points having majority and minority weights, respectively. The value in percentage corresponds to the weight of the Fourier component of the corresponding pattern on these  $k$  points for the temperature of 10 K in Phase 1, 335 K in Phase 2, 339 K in Phase 3, 341.5 K in Phase 4, and 370 K in Phase 5. Note also that the weight on  $\frac{2\pi}{a_{\text{lat}}}(0,0,\frac{1}{4})$  is identical to that on the opposite  $\frac{2\pi}{a_{\text{lat}}}(0,0,-\frac{1}{4})$   $k$  point for the pattern associated with the  $x$  component or  $y$  component of the local modes. Similarly, the eight  $k$  points defined by  $\frac{2\pi}{a_{\text{lat}}}(\pm\frac{1}{2}, \pm\frac{1}{n}, \pm\frac{1}{2})$  [respectively,  $\frac{2\pi}{a_{\text{lat}}}(\pm\frac{1}{2}, \pm\frac{1}{2}, \pm\frac{1}{n})$ ], with  $n$  being 4, 6, or 12, all have the same weight for the pattern inherent to the  $y$  component (respectively,  $z$  component) of the AFD pseudovectors.

State	$\mathbf{k}_{u,x}$	$\mathbf{k}_{u,y}$	$\mathbf{k}_{u,z}$	$\mathbf{k}_{\text{AFD},x}$	$\mathbf{k}_{\text{AFD},y}$	$\mathbf{k}_{\text{AFD},z}$
Phase 1	$(0,0,\frac{1}{4})$ , 48.2%	$(0,0,\frac{1}{4})$ , 48.2%	$\mathbf{0}$ (maj, 87.8%) $(0,0,\frac{1}{2})$ (min, 9.6%)	$(\frac{1}{2},\frac{1}{2},\frac{1}{2})$ , 99.8%	$(\frac{1}{2},\frac{1}{2},\frac{1}{2})$ , 99.8%	$(\frac{1}{2},\frac{1}{2},\frac{1}{4})$ , 49.9%
Phase 2	N/A	N/A	N/A	$(\frac{1}{2},\frac{1}{2},\frac{1}{2})$ , 45.5%	$(\frac{1}{2},\frac{1}{6},\frac{1}{2})$ (maj, 17.9%) $(\frac{1}{2},\frac{1}{4},\frac{1}{2})$ (min, 9.1%) $(\frac{1}{2},0,\frac{1}{2})$ (min, 7.5%)	$(\frac{1}{2},\frac{1}{2},\frac{1}{2})$ , 50.6%
Phase 3	N/A	N/A	N/A	N/A	$(\frac{1}{2},0,\frac{1}{2})$ (maj, 19.5%) $(\frac{1}{2},\frac{1}{4},\frac{1}{2})$ (min, 10.4%) $(\frac{1}{2},\frac{1}{6},\frac{1}{2})$ (min, 9.2%) $(\frac{1}{2},\frac{1}{12},\frac{1}{2})$ (min, 5.6%)	$(\frac{1}{2},\frac{1}{2},\frac{1}{2})$ , 52.6%
Phase 4	N/A	N/A	N/A	N/A	$(\frac{1}{2},0,\frac{1}{2})$ , 57.9%	$(\frac{1}{2},\frac{1}{2},\frac{1}{2})$ , 11.5%
Phase 5	N/A	N/A	N/A	N/A	$(\frac{1}{2},0,\frac{1}{2})$ , 71.9%	N/A

Another transition occurs at about 342 K, resulting in the vanishing of the antiphase tilting about the  $z$  axis and in the formation of Phase 5. Such a latter phase therefore adopts the rather simple  $a^0b^+a^0$  Glazer notation [68] and is the known  $T_2$  state of  $\text{NaNbO}_3$  [76] having the  $P4/mbm$  symmetry. This state is thus tetragonal, as consistent with the nonzero strain components depicted in Fig. 6. As shown in Fig. 9, the magnitude of the in-phase tilting is decreasing as the temperature increases from 342 K to 373 K, until Phase 5 transforms into the  $Pm\bar{3}m$  paraelectric cubic state (which is the so-called  $U$  state of  $\text{NaNbO}_3$  [12,14]) at this latter temperature.

One should also realize that the simulated transition temperatures are smaller than the experimental ones, as typical of effective Hamiltonian techniques for some systems [26], including  $\text{KNbO}_3$  [77] (one possible reason for such underestimation is discussed in Ref. [78]). For instance, the temperature of the transition from Phase 5 to  $Pm\bar{3}m$  is about 373 K in the MC computations while the corresponding transition from  $T_2$  to  $U$  occurs at about 914 K in measurements [76]. Similarly, the stability range of some phases is too small with respect to observations. For instance, our Phase 4 has only a temperature window of about 2 K while it is nearly 55 K in experiments for the corresponding  $T_1$  state [12–14]. On the other hand, it is rather remarkable that the currently developed effective Hamiltonian is not only able to find  $R3c$  to be the ground state of  $\text{NaNbO}_3$  (see Sec. III A) but also to correctly predict the existence of five other states (namely, Phases 1 to 5), with some of them being rather complex, in the phase transition sequence of  $\text{NaNbO}_3$ , before reaching  $Pm\bar{3}m$  at high temperature. It thus appears that this presently developed  $H_{\text{eff}}$  can rather well qualitatively describe the enormous complexity inherent to  $\text{NaNbO}_3$ . Let us thus take advantage of it, and more precisely of its parameters listed in Table I, to better understand subtle features of  $\text{NaNbO}_3$  that make such a compound deserving its nickname of “the most complicated perovskite system.”

We may also wonder which other perovskites systems can have effects that are similar to the ones described above, in general, and that can be well described by the analytical form of our developed effective Hamiltonian [see Eqs. (1)–(6)], in particular.

#### IV. DISCUSSION

For that, we will mostly proceed by asking questions that are not trivial in our minds and then will answer them by pointing out some specific important parameters of the effective Hamiltonian.

(1) *Why does  $\text{NaNbO}_3$  first adopt in-phase tilting rather than antiphase tilting when reducing the temperature from the cubic paraelectric state, that is in Phase 5?* The answer to this question, in fact, resides in the *negative* sign of the  $k_2$  AFD short-range parameter that does favor in-phase tilting with respect to antiphase tilting. A further proof of such fact is numerically found by increasing by hand the magnitude of this coefficient while keeping it negative. In that case, the temperature range of stability of Phase 5 gets enhanced with respect to the one shown in Figs. 6–9.

(2) *Why does  $\text{NaNbO}_3$  exhibit antiphase and/or complex tilting associated with the  $k$  point being halfway between the  $R$  and  $M$  points in its two lowest-in-energy phases (i.e.,  $R3c$  and Phase 1) at low temperature, while it prefers to exhibit in-phase tilting in the higher-temperature Phase 5?* As documented in Sec. III A, some subtle interactions (e.g., those involving  $E_{xyxy}$  and  $D_{ii,xy}$ ) coefficients between antiphase oxygen octahedral tiltings, the complex tilting inherent to  $\frac{2\pi}{a_{\text{lat}}}(\frac{1}{2},\frac{1}{2},\frac{1}{4})$  and cation displacements do help to stabilize, at low temperature,  $R3c$  and Phase 1—that do not possess in-phase tilting (unlike, e.g.,  $Pnma$ ).

(3) *Why do antipolar or polar motions only become important at low temperatures in  $\text{NaNbO}_3$ ?* As indicated in Table III, we only found that cation displacements are

long-range ordered in Phase 1, that is below 338 K in our calculations. Cation displacements are also seen in all the low-temperature (10 K) phases of Table II. The reason that such cation displacements do not play a large role at higher temperatures (e.g., in Phases 2–5) is that the internal energy of purely polar or antipolar phases is much smaller than that of pure AFD phases, as one can interfere from the rather small values of the coefficients entering Eq. (3) with respect to those appearing in the first four energetic terms of Eq. (5). For instance, we numerically found that the purely ferroelectric  $R3m$  state (that has a polarization along [111]) has an internal energy higher by an order of 0.1 eV/5 atom from the purely AFD  $R\bar{3}c$  state (that solely exhibits antiphase tilting about [111]) at 10 K, when using the  $H_{\text{eff}}$  parameters of Table I. Moreover, some interactions between cation displacements and AFD pseudovectors are repulsive in nature (see, e.g., the positive sign and large values of  $E_{xxx}$  and  $E_{xyy}$ ), therefore making the condensation of local modes even more difficult in some phases. On the other hand, once low-enough temperatures are reached and as aforementioned, some specific couplings between local modes and oxygen octahedral tiltings result in the stabilization of some phases exhibiting both cation displacements and AFD vectors.

(4) *Why does  $\text{NaNbO}_3$  exhibit nanotwins in Phases 2 and 3, that are characterized by some  $k$  vectors being in between the  $R$  and  $M$  points of the cubic first Brillouin zone but not equal to  $\frac{2\pi}{a_{\text{lat}}}(\frac{1}{2}, \frac{1}{2}, \frac{1}{4})$ ?* The competition between item (1) (favoring in-phase tilting) and item (2) (that wishes to make  $\text{NaNbO}_3$  possessing antiphase and/or the complex tiltings associated with  $\frac{2\pi}{a_{\text{lat}}}(\frac{1}{2}, \frac{1}{2}, \frac{1}{4})$  at low temperature) can make the system adopt a compromise and therefore have  $k$  points being in between the zone border  $M$  and  $R$  points but not equal to  $\frac{2\pi}{a_{\text{lat}}}(\frac{1}{2}, \frac{1}{2}, \frac{1}{4})$ . Such a possibility becomes even more probable when realizing that the  $k_2$  parameter of Table I is of very small magnitude, which automatically implies that the phonon branch bridging the  $R$  to  $M$  points in the cubic state is very flat. Note that such flatness has in fact been seen in previous works [81].

(5) *What other systems can be well described by the analytical form of the proposed effective Hamiltonian?* It is very likely that examples of such systems are  $\text{AgTaO}_3$  and  $\text{AgNbO}_3$ , because they are experimentally known to exhibit various similar complex phases [82–89]. Interestingly,  $\text{NaNbO}_3$ ,  $\text{AgTaO}_3$ , and  $\text{AgNbO}_3$  all share an almost identical tolerance factor, which is of the order of 0.97 (see Ref. [90] for the computation of the tolerance factor). Such a fact therefore suggests a strong connection between the existence of complex phases (and/or complicated phase transition sequence) and the value of the tolerance factor.

## V. SUMMARY

In summary, we have developed an effective Hamiltonian, and further used direct first-principles calculations, to shed some light into the extraordinary complexity of  $\text{NaNbO}_3$ . This effective Hamiltonian indicates that the ground state of  $\text{NaNbO}_3$  (which is the state called  $N$ ) is ferroelectric  $R\bar{3}c$  rather than purely simple or more complex tilting phases, because of some subtle and delicate couplings involving cation

displacements and oxygen octahedral tiltings. Moreover, both effective Hamiltonian computations and direct *ab initio* calculations predict that the so-called  $P$  state of  $\text{NaNbO}_3$  should be revisited, in the sense that it is likely of  $Pca2_1$  rather than  $Pbcm$  symmetry, and therefore has an additional (inhomogeneous) polarization along the [001] axis in addition to antiphase tilting about [110] and a “+ + – –” tilting pattern about the  $z$  axis when moving along any [001] line. Our simulations for the  $T_1$ ,  $T_2$ , and  $U$  states are consistent with some phases previously proposed in the literature, that are simple tilting pattern  $a^0b^+c^-$  and  $a^0b^+a^0$  for  $T_1$  and  $T_2$ , respectively, versus the paraelectric  $Pm\bar{3}m$  state for  $U$ . Moreover, our effective Hamiltonian computations also lead to the prediction of phases for the controversial  $R$  and  $S$  states, both of them being nanotwins of large periodicity along the long axis, namely 12-lattice constants in our case, and involving several  $k$  points for the complex tiltings occurring along such a long axis. Interestingly, the coexistence of several  $k$  points to fully describe complex tilting patterns has also been suggested in a recent article on Li-doped  $\text{NaNbO}_3$  compound [91].

Finally, by pointing out some specific important parameters of the effective Hamiltonian listed in Table I, we further elucidate nontrivial issues pertaining to the complexity of  $\text{NaNbO}_3$ . We therefore hope that this work leads to a revisiting and a better understanding of the most complex perovskite system and will encourage experimentalists to confirm some of our predictions. We also humbly but strongly believe that the present study firmly establishes that atomistic effective Hamiltonians are nowadays able to treat incredibly complicated compounds. They are therefore promising to tackle and understand other complex materials such as, e.g.,  $\text{AgTaO}_3$  [82–84] and  $\text{AgNbO}_3$  [85–89], and, for instance, explain why  $R\bar{3}c$  is the ground state of the former and not of the latter. Effective Hamiltonians can thus be used hand-in-hand with experimentalists in order to extract, confirm, and understand unusual phases from measured data. The presently developed effective Hamiltonian may also be put in use to study epitaxial films made of  $\text{NaNbO}_3$  in the hope of finding novel phases or phenomena [92].

## ACKNOWLEDGMENTS

This paper was supported by the National Natural Science Foundation of China (NSFC) (Grants No. 51672171, No. 51372149, and No. 11274222), the National Key Basic Research Program of China (Grant No. 2015CB921600), the Eastern Scholar Program from the Shanghai Municipal Education Commission and the fund of the State Key Laboratory of Solidification Processing in NWPU (Grant No. SKLSP201703). The Special Program for Applied Research on Super Computation of the NSFC-Guangdong Joint Fund (the second phase) and the China Scholarship Council are also acknowledged. B.X. and L.B. acknowledge the US AFOSR Grant No. FA9550-16-1-0065. C.X. thanks the Department of Energy, Office of Basic Energy Sciences, under Award # DE-SC0002220. The authors also acknowledge useful discussions with Drs. Philip Lightfoot and Charles Paillard. This paper is dedicated to Dr. Jean-Michel Kiat who enjoyed and mastered crystallography and tilting phases.

- [1] H. J. Zhao, J. Íñiguez, X. M. Chen, and L. Bellaiche, *Phys. Rev. B* **93**, 014417 (2016).
- [2] W. Ren, Y. Yang, O. Diéguez, J. Íñiguez, N. Choudhury, and L. Bellaiche, *Phys. Rev. Lett.* **110**, 187601 (2013).
- [3] R. J. Cava, B. Batlogg, J. J. Krajewski, R. Farrow, L. W. Rupp, Jr, A. E. White, K. Short, W. F. Peck, and T. Kometani, *Nature (London)* **332**, 814 (1988).
- [4] A. Stroppa, C. Quarti, F. De Angelis, and S. Picozzi, *J. Phys. Chem. Lett.* **6**, 2223 (2015).
- [5] M. E. Lines and A. M. Glass, *Principles and Applications of Ferroelectrics and Related Materials* (Clarendon Press, Oxford, 1977).
- [6] E. L. Falcão-Filho, C. A. C. Bosco, G. S. Maciel, L. H. Acioli, C. B. de Araújo, A. A. Lipovskii, and D. K. Tagantsev, *Phys. Rev. B* **69**, 134204 (2004).
- [7] J. H. Jung, M. Lee, J.-I. Hong, Y. Ding, C.-Y. Chen, L.-J. Chou, and Z. L. Wang, *ACS Nano* **5**, 10041 (2011).
- [8] Y. Saito, H. Takao, T. Tani, T. Nonoyama, K. Takatori, T. Homma, T. Nagaya, and M. Nakamura, *Nature (London)* **432**, 84 (2004).
- [9] J.-F. Li, K. Wang, F.-Y. Zhu, L.-Q. Cheng, F.-Z. Yao, and D. J. Green, *J. Am. Ceram. Soc.* **96**, 3677 (2013).
- [10] X. Wang, J. Wu, D. Xiao, J. Zhu, X. Cheng, T. Zheng, B. Zhang, X. Lou, and X. Wang, *J. Am. Chem. Soc.* **136**, 2905 (2014).
- [11] J. Wu, D. Xiao, and J. Zhu, *Chem. Rev.* **115**, 2559 (2015).
- [12] S. K. Mishra, R. Mittal, V. Y. Pomjakushin, and S. L. Chaplot, *Phys. Rev. B* **83**, 134105 (2011).
- [13] M. Ahtee, A. M. Glazer, and H. D. Megaw, *Philos. Mag.* **26**, 995 (1972).
- [14] H. D. Megaw, *Ferroelectrics* **7**, 87 (1974).
- [15] I. Lefkowitz, K. Lukaszewicz, and H. D. Megaw, *Acta Cryst.* **20**, 670 (1966).
- [16] L. A. Reznichenko, L. A. Shilkina, E. S. Gagarina, I. P. Raevskii, E. A. Dul'kin, E. M. Kuznetsova, and V. V. Akhnazarova, *Cryst. Rep.* **48**, 448 (2003).
- [17] L. M. Chao, Y. D. Hou, M. P. Zheng, and M. K. Zhu, *Appl. Phys. Lett.* **108**, 212902 (2016).
- [18] C. I. Cheon, H. W. Joo, K. W. Chae, J. S. Kim, S. H. Lee, S. Torii, and T. Kamiyama, *Mater. Lett.* **156**, 214 (2015).
- [19] S. I. Raevskaya, I. P. Raevski, S. P. Kubrin, M. S. Panchelyuga, V. G. Smotrakov, V. V. Eremkin, and S. A. Prosandeev, *J. Phys.: Condens. Matter* **20**, 232202 (2008).
- [20] I. Tomeno, Y. Tsunoda, K. Oka, M. Matsuura, and M. Nishi, *Phys. Rev. B* **80**, 104101 (2009).
- [21] L. Jiang, D. C. Mitchell, W. Dmowski, and T. Egami, *Phys. Rev. B* **88**, 014105 (2013).
- [22] S. K. Mishra, N. Choudhury, S. L. Chaplot, P. S. R. Krishna, and R. Mittal, *Phys. Rev. B* **76**, 024110 (2007).
- [23] U. V. Waghmare and K. M. Rabe, *Phys. Rev. B* **55**, 6161 (1997).
- [24] H. Krakauer, R. Yu, C.-Z. Wang, and C. LaSota, *Ferroelectrics* **206-207**, 133 (1998).
- [25] L. Bellaiche, A. García, and D. Vanderbilt, *Phys. Rev. Lett.* **84**, 5427 (2000).
- [26] W. Zhong, D. Vanderbilt, and K. M. Rabe, *Phys. Rev. Lett.* **73**, 1861 (1994); *Phys. Rev. B* **52**, 6301 (1995).
- [27] I. Grinberg, V. R. Cooper, and A. M. Rappe, *Nature (London)* **419**, 909 (2002).
- [28] I. Grinberg, V. R. Cooper, and A. M. Rappe, *Phys. Rev. B* **69**, 144118 (2004).
- [29] S. Liu, I. Grinberg, H. Takenaka, and A. M. Rappe, *Phys. Rev. B* **88**, 104102 (2013).
- [30] M. G. Stachiotti and R. L. Migoni, *J. Phys.: Condens. Matter* **2**, 4341 (1990).
- [31] M. G. Stachiotti, R. L. Migoni, and U. T. Höchli, *J. Phys.: Condens. Matter* **3**, 3689 (1991).
- [32] S. Koval, M. G. Stachiotti, R. L. Migoni, M. S. Moreno, R. C. Mercader, and E. L. Peltzery Blancá, *Phys. Rev. B* **54**, 7151 (1996).
- [33] P. García-Fernández, J. C. Wojdeł, J. Íñiguez, and J. Junquera, *Phys. Rev. B* **93**, 195137 (2016).
- [34] C. Escorihuela-Sayalero, J. C. Wojdeł, and J. Íñiguez, *Phys. Rev. B* **95**, 094115 (2017).
- [35] B. Noheda, D. E. Cox, G. Shirane, J. A. Gonzalo, L. E. Cross, and S.-E. Park, *Appl. Phys. Lett.* **74**, 2059 (1999).
- [36] I. Kornev, H. Fu, and L. Bellaiche, *Phys. Rev. Lett.* **93**, 196104 (2004).
- [37] S. K. Streiffer, J. A. Eastman, D. D. Fong, C. Thompson, A. Munkholm, M. V. Ramana Murty, O. Auciello, G. R. Bai, and G. B. Stephenson, *Phys. Rev. Lett.* **89**, 067601 (2002).
- [38] D. D. Fong, G. B. Stephenson, S. K. Streiffer, J. A. Eastman, O. Auciello, P. H. Fuoss, and C. Thompson, *Science* **304**, 1650 (2004).
- [39] I. I. Naumov, L. Bellaiche, and H. Fu, *Nature (London)* **432**, 737 (2004).
- [40] Bo-Kuai Lai, I. Ponomareva, I. I. Naumov, I. A. Kornev, Huaxiang Fu, L. Bellaiche, and G. J. Salamo, *Phys. Rev. Lett.* **96**, 137602 (2006).
- [41] A. K. Yadav, C. T. Nelson, S. L. Hsu, Z. Hong, J. D. Clarkson, C. M. Schlepütz, A. R. Damodaran, P. Shafer, E. Arenholz, L. R. Dedon, D. Chen, A. Vishwanath, A. M. Minor, L. Q. Chen, J. F. Scott, L. W. Martin, and R. Ramesh, *Nature (London)* **530**, 198 (2016).
- [42] Q. Zhang, L. Xie, G. Liu, S. Prokhorenko, Y. Nahas, X. Pan, L. Bellaiche, A. Gruverman, and N. Valanoor, *Adv. Mater.* **29**, 1702375 (2017).
- [43] I. A. Kornev, L. Bellaiche, P. E. Janolin, B. Dkhil, and E. Suard, *Phys. Rev. Lett.* **97**, 157601 (2006).
- [44] S. Prosandeev, D. Wang, W. Ren, J. Íñiguez, and L. Bellaiche, *Adv. Funct. Mater.* **23**, 234 (2013).
- [45] D. Albrecht, S. Lisenkov, W. Ren, D. Rahmedov, I. A. Kornev, and L. Bellaiche, *Phys. Rev. B* **81**, 140401 (2010).
- [46] I. A. Kornev, S. Lisenkov, R. Haumont, B. Dkhil, and L. Bellaiche, *Phys. Rev. Lett.* **99**, 227602 (2007).
- [47] S. Lisenkov, I. A. Kornev, and L. Bellaiche, *Phys. Rev. B* **79**, 012101 (2009).
- [48] P. Hohenberg and W. Kohn, *Phys. Rev.* **136**, B864 (1964); W. Kohn and L. J. Sham, *ibid.* **140**, A1133 (1965).
- [49] L. Bellaiche and D. Vanderbilt, *Phys. Rev. B* **61**, 7877 (2000).
- [50] D. Vanderbilt, *Phys. Rev. B* **41**, 7892 (1990).
- [51] R. D. King-Smith and D. Vanderbilt, *Phys. Rev. B* **49**, 5828 (1994).
- [52] J. P. Perdew, A. Ruzsinszky, G. I. Csonka, O. A. Vydrov, G. E. Scuseria, L. A. Constantin, X. Zhou, and K. Burke, *Phys. Rev. Lett.* **100**, 136406 (2008).
- [53] R. Machado, M. Sepliarsky, and M. G. Stachiotti, *Phys. Rev. B* **84**, 134107 (2011).

- [54] R. Von der Mühl, A. Sadel, and P. Hagenmuller, *J. Solid State Chem.* **51**, 176 (1984).
- [55] M. D. Peel, S. P. Thompson, A. Daoud-Aladine, S. E. Ashbrook, and P. Lightfoot, *Inorg. Chem.* **51**, 6876 (2012).
- [56] A. C. Sakowski-Cowley, K. Lukaszewicz, and H. D. Megaw, *Acta Cryst. B* **25**, 851 (1969).
- [57] G. Kresse and D. Joubert, *Phys. Rev. B* **59**, 1758 (1999).
- [58] P. E. Blochl, *Phys. Rev. B* **50**, 17953 (1994).
- [59] G.-R. Qian, X. Dong, X.-F. Zhou, Y. Tian, A. R. Oganov, and H.-T. Wang, *Comput. Phys. Commun.* **184**, 2111 (2013).
- [60] A. R. Oganov and C. W. Glass, *J. Chem. Phys.* **124**, 244704 (2006).
- [61] A. R. Oganov, A. O. Lyakhov, and M. Valle, *Acc. Chem. Res.* **44**, 227 (2011).
- [62] A. O. Lyakhov, A. R. Oganov, H. T. Stokes, and Q. Zhu, *Comput. Phys. Commun.* **184**, 1172 (2013).
- [63] X. Gonze, G.-M. Rignanese, M. Verstraete, J.-M. Beuken, Y. Pouillon, R. Caracas, F. Jollet, M. Torrent, G. Zerah, M. Mikami, Ph. Ghosez, M. Veithen, J.-Y. Raty, V. Olevano, F. Bruneval, L. Reining, R. Godby, G. Onida, D. R. Hamann, and D. C. Allan, *Z. Kristallogr.* **220**, 558 (2005).
- [64] X. Gonze, B. Amadon, P.-M. Anglade, J.-M. Beuken, F. Bottin, P. Boulanger, F. Bruneval, D. Caliste, R. Caracas, M. Côté, T. Deutsch, L. Genovese, Ph. Ghosez, M. Giantomassi, S. Goedecker, D. R. Hamann, P. Hermet, F. Jollet, G. Jomard, S. Leroux, M. Mancini, S. Mazevet, M. J. T. Oliveira, G. Onida, Y. Pouillon, T. Rangel, G.-M. Rignanese, D. Sangalli, R. Shaltaf, M. Torrent, M. J. Verstraete, G. Zerah, and J. W. Zwanziger, *Comput. Phys. Commun.* **180**, 2582 (2009).
- [65] X. Gonze, F. Jollet, F. Abreu Araujo, D. Adams, B. Amadon, T. Applencourt, C. Audouze, J.-M. Beuken, J. Bieder, A. Bokhanchuk, E. Bousquet, F. Bruneval, D. Caliste, M. Côté, F. Dahm, F. Da Pieve, M. Delaveau, M. Di Gennaro, B. Dorado, C. Espejo, G. Geneste, L. Genovese, A. Gerossier, M. Giantomassi, Y. Gillet, D. R. Hamann, L. He, G. Jomard, J. Laflamme Janssen, S. Le Roux, A. Levitt, A. Lherbier, F. Liu, I. Lukacevic, A. Martin, C. Martins, M. J. T. Oliveira, S. Poncé, Y. Pouillon, T. Rangel, G.-M. Rignanese, A. H. Romero, B. Rousseau, O. Rubel, A. A. Shukri, M. Stankovski, M. Torrent, M. J. Van Setten, B. Van troeye, M. J. Verstraete, D. Waroquier, J. Wiktor, B. Xu, A. Zhou, and J. W. Zwanziger, *Comput. Phys. Commun.* **205**, 106 (2016).
- [66] D. R. Hamann, *Phys. Rev. B* **88**, 085117 (2013).
- [67] C. N. W. Darlington and H. D. Megaw, *Acta Cryst. B* **29**, 2171 (1973).
- [68] A. M. Glazer, *Acta Cryst. B* **28**, 3384 (1972).
- [69] O. Diéguez, O. E. González-Vázquez, J. C. Wojdel, and J. Íñiguez, *Phys. Rev. B* **83**, 094105 (2011).
- [70] L. Bellaïche and J. Íñiguez, *Phys. Rev. B* **88**, 014104 (2013).
- [71] A. M. George, J. Íñiguez, and L. Bellaïche, *Phys. Rev. B* **65**, 180301(R) (2002).
- [72] B. N. Rao, D. K. Khatua, R. Garg, A. Senyshyn, and R. Ranjan, *Phys. Rev. B* **91**, 214116 (2015).
- [73] W. L. Zhong, P. L. Zhang, H. S. Zhao, Z. H. Yang, Y. Y. Song, and H. C. Chen, *Phys. Rev. B* **46**, 10583 (1992).
- [74] A. C. Sakowski-Cowley, Ph.D. Thesis, University of Cambridge (1967).
- [75] Y. I. Yuzyuk, P. Simon, E. Gagarina, L. Hennem, D. Thiaudière, V. I. Torgashev, S. I. Raevskaya, I. P. Raevskii, L. A. Reznitchenko, and J. L. Sauvajol, *J. Phys.: Condens. Matter* **17**, 4977 (2005).
- [76] A. M. Glazer and H. D. Megaw, *Philos. Mag.* **25**, 1119 (1972).
- [77] H. Krakauer, R. Yu, C.-Z. Wang, K. M. Rabe and U. V. Waghmare, *J. Phys.: Condens. Matter* **11**, 3779 (1999).
- [78] One may wonder what is the origin of the underestimation of transition temperatures from the effective Hamiltonian method. One possible reason is that the main degrees of freedom of  $\text{KNbO}_3$  and  $\text{NaNbO}_3$  (namely, local electric dipoles and local oxygen octahedral tiltings, respectively) may couple, in a *collaborative* fashion, with other degrees of freedom. Such latter degrees of freedom never condense at any temperature but can fluctuate at high temperatures, with such fluctuations and aforementioned collaborative coupling resulting in the main degrees of freedom of  $\text{KNbO}_3$  and  $\text{NaNbO}_3$  surviving at higher temperatures. As a result, neglecting this coupling in our effective Hamiltonian, as done here, can lead to an underestimation of the transition temperatures while providing the correct phase transition sequence. Note that such possible aforementioned coupling [79] is consistent with recent measurements showing the manipulation of the polarization in  $\text{LiNbO}_3$  via light-induced excitation of high-in-frequency modes [80].
- [79] A. Subedi, *Phys. Rev. B* **92**, 214303 (2015).
- [80] R. Mankowsky, A. von Hoegen, M. Forst, and A. Cavalleri, *Phys. Rev. Lett.* **118**, 197601 (2017).
- [81] S. K. Mishra, M. K. Gupta, R. Mittal, M. Zbiri, S. Rols, H. Schober, and S. L. Chaplot, *Phys. Rev. B* **89**, 184303 (2014).
- [82] M. Wołczyr and M. Łukaszewski, *Z. Kristallogr.* **177**, 53 (1986).
- [83] G. E. Kugel, M. D. Fontana, M. Hafid, K. Roleder, A. Kania, and M. Pawelczyk, *J. Phys. C* **20**, 1217 (1987).
- [84] A. Kania and A. Ratuszna, *Phase. Transit.* **2**, 7 (1981).
- [85] I. Grinberg and A. M. Rappe, *AIP Conf. Proc.* **677**, 130 (2003).
- [86] P. Sciau, A. Kania, B. Dkhil, E. Suard, and A. Ratuszna, *J. Phys.: Condens. Matter* **16**, 2795 (2004).
- [87] I. Levin, V. Krayzman, J. C. Woicik, J. Karapetrova, T. Proffen, M. G. Tucker, and I. M. Reaney, *Phys. Rev. B* **79**, 104113 (2009).
- [88] M. Yashima, S. Matsuyama, R. Sano, M. Itoh, K. Tsuda, and D. Fu, *Chem. Mater.* **23**, 1643 (2011).
- [89] M. Hiroki, A. J. F. Craig, K. Akihida, and F. Desheng, *Jpn. J. Appl. Phys.* **51**, 09LE02 (2012).
- [90] <http://www.me.utexas.edu/~benedekgroup/ToleranceFactorCalculator/#home>.
- [91] C. A. L. Dixon and P. Lightfoot, [arXiv:1802.08493](https://arxiv.org/abs/1802.08493).
- [92] Y. Yang, W. Ren, M. Stengel, X. H. Yan, and L. Bellaïche, *Phys. Rev. Lett.* **109**, 057602 (2012).